Injury mechanism in non-penetrating thoracic impact: finite element study

Quentin Grimal* — **Salah Naïli****

** Laboratoire d'Imagerie Paramétrique, UMR CNRS 7623*
Université Pierre et Marie Curie
15, rue de l'école de médecine
F-75006 Paris

quentin.grimal@lip.bhdc.jussieu.fr

*** Laboratoire de Mécanique Physique, CNRS UMR 7052 B2OA*
Université Paris XII-Val de Marne, Faculté des Sciences et Technologie
61, Avenue du Général de Gaulle
F-94010 Créteil Cedex

naili@univ-paris12.fr

ABSTRACT. *The work presented is motivated especially by behind armor blunt trauma, that is, injury following the defeat of a high-energy projectile by a rigid body armor. While the bullet is stopped and the effects of the projectile penetrating the biological tissues are prevented, a considerable amount of energy is transmitted through the projective layers of the armor, and delivered to the human body. Eventually, tissues behind the body armor are injured. An idealized model of the thorax (thoracic wall and lung) was built. The dynamic response of the thorax model is calculated. The results presented allow to describe a probable injury mechanism.*

RÉSUMÉ. *Le travail présenté est spécialement motivé par les traumatismes susceptibles de se produire derrière une protection de type gilet pare-balles, c'est-à-dire les lésions observées suite à l'impact non pénétrant d'un projectile haute énergie. Tandis que le projectile est arrêté par la protection, une quantité considérable de l'énergie est transmise au corps humain. Les tissus derrière la protection sont alors susceptibles d'être lésés. Les réponses dynamiques de la paroi thoracique et du poumon sont calculées. Ces résultats permettent de décrire un mécanisme probable des lésions.*

KEYWORDS: *biomechanics, impact, blunt trauma, finite elements.*

MOTS-CLÉS : *biomécanique, impact, traumatisme brutal, éléments finis.*

REFF – 14/2005. Biomechanics of impact, pages 517 to 540

1. Introduction

The lung is an organ often damaged in high-velocity loading situations. Although the detailed damage mechanisms leading to lung injury (edema or hemorrhage in the alveoli) are still unclear, it is well established that this specific fragility of the lung is in close relation to its high compliance (Fung, 1990).

Waves in the lung travel at very low velocities. This velocity has been measured in a number of studies and great dispersion on the velocities values have been found. These range from a few meters per seconds up to a few hundreds meters per second. The dispersion is due to the measurement protocols, for instance, the velocity depends on how much air is in the lung and whether or not waves travelling at the surface of the organ are considered. Wave velocities of 40 m s^{-1} is common. As a consequence of the low wave velocities, the wavelengths of the waves propagated in the lung are much smaller than in other organs or tissues (heart, bone, etc.) for a given mechanical loading. Hence in many loading conditions wave phenomena are expected to be paramount in the lung, while not in other organs. Accordingly, many authors have conjectured that lung damage is due to the propagation of a *wave* (Bush *et al.*, 1988; Yen *et al.*, 1988; Fung, 1990), *i.e.*, that lung injury is generated by a "high-frequency" injury mechanism.

Extended damage in the lung has been reported in the following situations. Body exposure to blast ("blast loading") (Cooper *et al.*, 1991; Stuhmiller *et al.*, 1988); impact on thorax of projectiles used with non-lethal kinetic weapons (Cooper *et al.*, 1982; Cooper *et al.*, 1986; Bir, 2000); sports (baseball, hockey); projectile defeated by a body armor. The work reported in this paper was motivated specifically by the latter: behind armor blunt trauma (BABT), that is, injury following the defeat of a high-energy projectile (typically 3500 J generated by impact of a 7.62 mm NATO bullet at 800 m s^{-1}) by a rigid body armor. In the past five years, research teams taking part in a NATO task group on BABT have generated most of the knowledge on the subject, see for instance the references Sarron *et al.* (2000), van Bree *et al.* (2000) and Raftenberg (2003) in the open literature.

The response of the thorax protected by a rigid body armor to impact by a high energy projectile is a sequence of two phenomena, observed successively (van Bree *et al.*, 2000; Cooper *et al.*, 1982; Cooper *et al.*, 1991): (1) a high-frequency response associated with *small displacements* of the tissues, followed by (2) a low-frequency response, namely, a large distorsion of the thoracic wall. Corresponding to these two parts of the loading, high- and low-frequency injury mechanisms can be described.

Until now, no experiment could demonstrate without ambiguity which of high- or low-frequency injury mechanisms are the most dangerous. While cardiac contusions, rib fractures and pulmonary injuries related to rib fracture or rib motion are likely low-frequency (*i.e.*, localized lung injury is likely a high-frequency injury mechanism).

The objective of modelling the thorax response to impact is to help predict which of these injuries is actually met after a given impact and its importance, in terms of

threat to life, relative to others injuries. These depend on many parameters, among which are the location of the impact, size of projectile and, most importantly, frequency content of the impact impulse.

This work reports a finite element study of the thoracic wall high-frequency response. We have considered a very short loading duration, between 50 μs and 300 μs typical in BABT impact experiments. The mechanism of energy transfer to internal organs during the high-frequency response has been described as follows (van Bree *et al.*, 2000): the contact of the bullet on the face of the rigid body armor generates a very short duration stress wave which propagates through the armor and enters directly into the body; no significant motion of the body wall is observed during the passage of the wave. The low-frequency response of the thorax is not considered in the present study.

As far as we know, modeling of the high-frequency response has not been conducted in the past, in contrast to the low-frequency response which have been addressed by several research teams (Raftenberg, 2003; Sarron *et al.*, 2000). Various FE models have been used to predict injuries in automobile accidents (Viano *et al.*, 1989; Wang, 1995), with the complexity of the models increasing over the past decades. Due to the different impact mechanics of automobile accidents and bullet impact on body armor, state of the art models used by the automobile industry cannot be used straightforward to study BABT. In particular material data measured in the specific loading conditions encountered in BABT problems are not available. Furthermore, the meshes currently used are too coarse to account for wave phenomena. The use of FE models in BABT is quite recent (Sarron *et al.*, 2000; Raftenberg *et al.*, 2001; Bush *et al.*, 1988). Existing FE models for the simulation of BABT mostly use linearly elastic material properties. Raftenberg *et al.* (2001) (and Raftenberg (2003)) used a FE model developed at the Wayne State University (Wang, 1995) for the simulation of automobile accidents. In their study, most of the thoracic tissues were modeled as isotropic with linearly elastic constitutive laws based on quasi-static experimental data. Only the lung and the heart were modeled with nonlinear behaviours (Vawter *et al.*, 1979; Vawter, 1980)), with stiffness increasing with increasing strain. This BABT model is at the validation stage (Raftenberg, 2003) but it seems unable to compute the propagation of the high-frequency response because of a coarse mesh.

With this review as background, Section 2 presents the model of the thorax, Section 3 is dedicated to the FE method of solution. Results are presented in Section 4 and discussed in Section 5.

2. Method

2.1. *Model geometry*

The geometry of the model, shown in Figure 1, is a layered medium which is bounded by a free surface, and which is otherwise of unlimited extent; the layered structure was inspired by cryosections of the human thorax (see Visible Human

Project, (National Library of Medicine, 2003)). Interfaces between layers are planes. Layers 1 and 2 represent the thoracic wall (TW) and layer 3 represents the lung. The tissues of the TW taken into account are muscle (layer 1) and bones (layer 2).

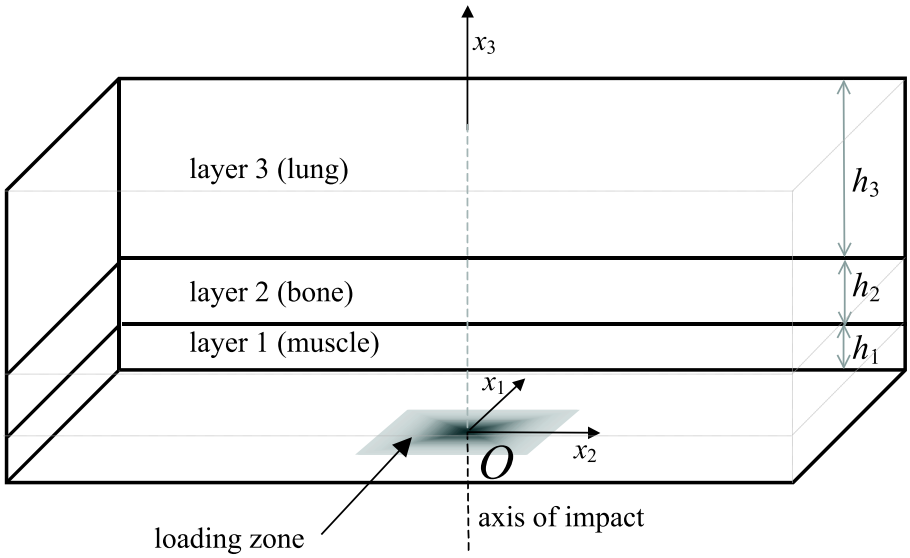

Figure 1. *Geometrical configuration of the model*

The three-layer model is a major simplification from the real thorax structure: no fat is taken into account, nor the detailed geometry of the ribs, nor organs others than the lung. With this model, the study is necessarily limited to a zone close beneath the impact point; the propagation of energy in the whole thorax is not considered. It is possible to obtain realistic results with such a model only in a narrow time window; results loose physical meaning when a sufficient part of the energy transmitted to the thorax has propagated away from the impact point, where tissues of the thorax (heart, ribs, spine, etc ... not taken into account in the model) start playing a role in the response. In the present study where the response is analyzed close to the impact point and in a short time window after the impact, it is sufficient to model only a small part of the thorax structure.

Afterwards, each layer will be denoted by Ω_r (r = 1, 2, 3) and the parallelepiped formed by the assembly of the three layers by Ω. The lateral surface of Ω will denoted by $\partial\Omega$. The interface between layers 1 and 2 will be designated by Σ_1 and the one between layers 2 and 3 by Σ_2. The boundary located at the bottom face of layer 1 will be stood for $\partial_1\Omega$ and the one located at the upper face of layer 3 by $\partial_2\Omega$.

Let M be a particle of Ω located at point $\mathbf{x}$. Its coordinates are denoted by x_i (i = 1, 2, 3) in the Cartesian framework $\mathbf{R}$ (O; $\mathbf{x}_1$, $\mathbf{x}_2$, $\mathbf{x}_3$), where O is the origin and ($\mathbf{x}_1$, $\mathbf{x}_2$, $\mathbf{x}_3$) is the orthogonal basis for the space. Vector $\mathbf{x}_3$ is taken perpendicular

to the interfaces. The thickness of the layers are denoted by h_r (r = 1, 2, 3). For the purpose of the finite element (FE) discretization, all the dimensions of the model must be finite; the dimensions in the $\mathbf{x}_1$ and $\mathbf{x}_2$ directions, as well as h_3 are chosen so that, within the time window of the computation, the waves reflected at the boundaries do not have the time to travel back to the location of interest (*i.e.*, a few centimeters around the axis $(O; \mathbf{x}_3)$).

The model dimensions and the thickness of the layers are respectively given in section 3.1 and in Table 1

2.2. *Governing equations*

Let $\mathbf{u}(\mathbf{x}, t)$ and $\mathbf{v}(\mathbf{x}, t)$ be respectively the displacement and the velocity at time t of a particle located at point $\mathbf{x}$ in Ω. For any function $a(\mathbf{x}, t)$, we use the notation $a_{,j}(\mathbf{x}, t) = \partial a(\mathbf{x}, t)/\partial x_j$ and $\partial_t a(\mathbf{x}, t) = \partial a(\mathbf{x}, t)/\partial t$. The velocity particle is defined from the particle displacement by $\mathbf{v}(\mathbf{x}, t) = \partial_t \mathbf{u}(\mathbf{x}, t)$. The components of the vector $\mathbf{u}(\mathbf{x}, t)$ are denoted by u_i in $\mathbf{R}$. The Cauchy stress tensor is designated by $\boldsymbol{\sigma}(\mathbf{x}, t)$ and these components by σ_{ij} in $\mathbf{R}$.

The governing equation of the motion of each Ω_r (r = 1, 2, 3) is derived from the momentum conservation in which the body force is neglected, so-called elastodynamic equation

$$\mathbf{div}\,\boldsymbol{\sigma}(\mathbf{x}, t) = \rho\,\partial_t \mathbf{v}(\mathbf{x}, t), \quad \text{in } \Omega_r \text{ and for } \; t > 0 \qquad [1]$$

where ρ is the mass density and the operator **div** designates the divergence.

The linearized symmetric strain tensor $\boldsymbol{\epsilon}(\mathbf{x}, t)$ is related to displacement field $\mathbf{u}$ by

$$\boldsymbol{\epsilon} = \frac{1}{2}\left(\mathbf{grad}\,\mathbf{u} + (\mathbf{grad}\,\mathbf{u})^T\right), \qquad [2]$$

where the gradient operator is denoted by **grad** and the transpose operator by $(.)^T$.

The problem consists in seeking a solution for (1) satisfying boundary, interface and initial conditions given in section 2.4.

2.3. *Constitutive law and material properties*

Although it is well-known that biological materials are viscous and nonlinear, there is very little experimental data available relevant for studies of high-velocity impact loadings. Hence, in accordance with previous studies of BABT related problems (Raftenberg, 2003), the material constitutive laws for the three layers are assumed homogeneous, isotropic and linearly elastic. A Poisson's ratio, denoted by ν, and a Young's modulus, denoted by E, are attributed to each layer.

The stress tensor $\boldsymbol{\sigma}$ is related to the strain tensor $\boldsymbol{\epsilon}$ by the constitutive law, so-called Hooke law

$$\boldsymbol{\sigma} = \frac{E\nu}{(1+\nu)(1-2\nu)}(\text{Tra}\,\boldsymbol{\epsilon})\mathbf{I} + \frac{E}{(1+\nu)}\boldsymbol{\epsilon}, \qquad [3]$$

where the tensor identity is denoted by $\mathbf{I}$ and the trace operator by Tra.

The longitudinal and shear wave speeds are denoted, respectively, by c_L and c_S

$$c_L = \sqrt{\frac{E(1-\nu)}{(1+\nu)(1-2\nu)\rho}}, \quad c_S = \sqrt{\frac{E}{2(1+\nu)\rho}}. \qquad [4]$$

The material properties are given in Table 1. Because of the extensive use of ultrasound (US) techniques in biology, wave speeds in various tissues for high frequency waves (a few megahertz) are well known. For the impact wave problem investigated in the present study, the particle displacements in the tissues are small, which is a common feature with US loading of tissues; hence the mechanical parameters for the constitutive laws derived from US experimental data were used. A common value used in US application for muscle is c_L=1600 m s^{-1} (which is consistent with the propagation velocity of waves in water); the muscle being mainly composed of water, density and Poisson's ratio are chosen to be, respectively, ρ=1000 kg m^{-3} and ν=0.45 (accounting for the poor compressibility of muscle). Some computations, not presented here, have shown that the response of the thorax model for the loading cases of the present study is weakly dependent on the value of the Poisson's ratio. The mechanical behavior of bone is well-suited to a linearly elastic model (Fung, 1993); we have used the same values as Wang (1995) and Raftenberg *et al.* (2001). As for the lung, much literature can be found on wave propagation (Yen *et al.*, 1986; Jahed *et al.*, 1989); the values for pressure and shear waves vary from one study to another due to experimental conditions. In agreement with the longitudinal and shear wave speeds measured in the lung by Jahed *et al.* (1989), we have used c_L=40 m s^{-1} and c_S=21 m s^{-1}; with the density taken to be ρ=600 kg m^{-3}. Finally, the parameters of constitutive law for the lung are derived from the density and the wave speeds.

Table 1. *Mechanical and geometrical characteristics of the layers*

	layer 1 (Muscle)	layer 2 (Bone)	layer 3 (Lung)
E (GPa)	0.675	11	0.713×10^{-3}
ν	0.45	0.3	0.3
ρ (kg m^{-3})	1000	2000	600
c_L (m s^{-1})	1600	2721	40
c_S (m s^{-1})	482	1454	21
h (cm)	0.5	1.5	2

2.4. *Boundary, interface and initial conditions*

Layers 1 and 2 are in welded contact, *i.e.*, the normal stresses and the displacements are continuous across the interface.

The lung and the thoracic wall are separated by a small potential space–the pleural cavity–which contains a lubricating fluid allowing the media to move easily on each other; in addition, under normal physiological conditions, pressure in the cavity is below atmospheric pressure so that the media remain in contact. Given this description of the biological structure, the simplest realistic model of contact at the thoracic wall-lung interface is frictionless sliding. As far we know, there is no experimental data that could be used to implement a model of friction with contact. Hence a model of frictionless contact is used at the interface between layer 2 and 3.

Let $\mathbf{n}$ be the unit normal vector to $\partial\Omega$ and external to Ω. For r = 1, 2, 3, $\mathbf{n}^r$ is the unit normal vector to the boundary of Ω_r and external to Ω_r. Moreover, $\boldsymbol{\sigma}^r$ and $\mathbf{u}^r$ are the restriction of the stress tensor and the displacement fields to Ω_r respectively. The boundary and interface conditions are given by

$$\begin{cases} \boldsymbol{\sigma}\mathbf{n} = \mathbf{0} & \text{on } \partial\Omega \\ \boldsymbol{\sigma}^1\mathbf{n}^1 = \mathbf{G} & \text{on } \partial_1\Omega \\ \boldsymbol{\sigma}^2\mathbf{n}^2 = \mathbf{0} & \text{on } \partial_2\Omega \\ \boldsymbol{\sigma}^1\mathbf{n}^1 = -\boldsymbol{\sigma}^2\mathbf{n}^2 & \text{on } \Sigma_1 \\ \mathbf{u}^1 = \mathbf{u}^2 & \text{on } \Sigma_1 \\ (\boldsymbol{\sigma}^1\mathbf{n}^1)\mathbf{n}^1 = -(\boldsymbol{\sigma}^2\mathbf{n}^2)\mathbf{n}^2 & \text{on } \Sigma_2 \\ \mathbf{T}^2 - (\mathbf{T}^2\mathbf{n}^2)\mathbf{n}^2 = \mathbf{0} & \text{on } \Sigma_2 \\ \mathbf{T}^3 - (\mathbf{T}^3\mathbf{n}^3)\mathbf{n}^3 = \mathbf{0} & \text{on } \Sigma_2 \\ \mathbf{u}^2\mathbf{n}^2 = -\mathbf{u}^3\mathbf{n}^3 & \text{on } \Sigma_2 \end{cases} \quad [5]$$

where $\mathbf{T}^r = \boldsymbol{\sigma}^r\mathbf{n}^r$ is the stress vector.

It is a difficult task to model the whole impact problem: impact of bullet on body armor, propagation of impact energy through the armor and propagation of energy through the thorax. Raftenberg (2003) chose to model the whole problem and this implies to make many assumptions on the mechanisms of dissipation of energy inside the armor. In contrast, in present work the armor is not modeled; the interaction of the armor with the body is represented by given boundary conditions on the thoracic wall surface. Hence this work is based on the hypothesis that the propagation of energy inside the thorax can be regarded as a problem independent of the transmission of energy in the body armor, once the pressure distribution on the surface of the TW is known. A similar approach was used by Sarron *et al.* (2000) (and Sarron (2001)) for the modeling of the low-frequency thorax response. In this study, the loading $\mathbf{G}$ consists in a time dependant pressure applied on the external surface of $\partial_1\Omega$. Experimental data was used to determine the loading; the complete description of the loading is postponed to section 3.3.1.

All the layers are at rest before the beginning of the computations. The initial conditions are given by

$$\mathbf{u}(\mathbf{x},0)=\mathbf{0}\,,\quad \mathbf{v}(\mathbf{x},0)=\mathbf{0}. \qquad [6]$$

Note that the structure Ω is free, then the general solution of the system of equations is given by

$$\mathbf{u}_{\text{rig}}(\mathbf{x},t)=\mathbf{t}+\boldsymbol{\theta}\wedge\mathbf{x},\quad \forall\mathbf{x}\in\Omega, \qquad [7]$$

in which $\mathbf{t}$ and $\boldsymbol{\theta}$ are two arbitrary constant vectors. The symbol $\wedge$ designates the vector product. The vector $\mathbf{u}_{\text{rig}}$ represents the rigid body displacement field. This rigid body displacement did not affect the results.

3. Numerical method and computations

3.1. *Mesh*

The planes (O, $\mathbf{x}_1$, $\mathbf{x}_3$) and (O, $\mathbf{x}_2$, $\mathbf{x}_3$) are planes of symmetry for the model geometry; in the FE representation, only one fourth of the geometry is modeled and appropriate boundary conditions are set on the symmetry planes. Hexahedral elements with 8-nodes were used. Since in the present study, only the response close to the $\mathbf{x}_3$-axis is of interest, a graduated mesh in the $\mathbf{x}_1$ and $\mathbf{x}_2$ directions in order to reduce the total number of elements was used. A typical mesh used for the computations is shown in Figure 2. A parallelepiped of dimension 80 cm×80 cm×4 cm is meshed with a total of 83,780 elements and 90,800 nodes.

3.2. *Numerical solution of the governing equations*

The finite element discretization of equations obtained from the variational formulation of Eqs. (1) associated with the boundary and interface conditions given by Eqs. (5) lead to the matrix initial-value problem

$$\begin{aligned}&\mathbf{M}\ddot{\mathbf{U}}+\mathbf{K}\mathbf{U}=\mathbf{F},\quad t\in\,]0,T_t]\\&\mathbf{U}(0)=\mathbf{0},\quad \dot{\mathbf{U}}(0)=\mathbf{0},\end{aligned} \qquad [8]$$

where $\mathbf{U}$, $\dot{\mathbf{U}}$ and $\ddot{\mathbf{U}}$ designate respectively the displacement, velocity and acceleration vectors of the finite element assemblage. The vector $\mathbf{F}$ corresponds to the finite element discretization of the given force. The mass and stiffness matrices are designated by $\mathbf{M}$ and $\mathbf{K}$ respectively. The termination time is denoted by T_t.

To obtain this system, the one point volume integration formula (LS-DYNA default) associated with the hexahedral elements was used; the use of more accurate integration formulas offered no improvement in accuracy for the mesh used in this study.

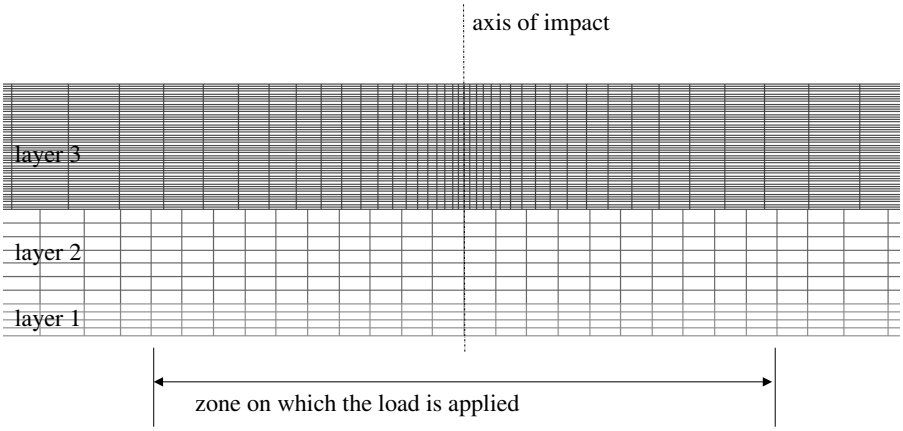

Figure 2. *Mesh used in the computations. Only a small part of the structure in the lateral direction is represented*

The computation of the transient response of the structure with the LS-DYNA software is possible by an explicit or implicit time integration method. Because the transient response must be calculated sufficiently accurately in the relatively small time window the explicit method is chosen. Indeed, an accurate description of the transient response assumes a small time step which is necessary when the explicit method is used. Moreover, the explicit time integration scheme in the LS-DYNA is known to be efficient in structures where the analysis of contact is required.

The central difference method is used to approach $\ddot{\mathbf{U}}$ and $\dot{\mathbf{U}}$. The discretization error is $O(\Delta t^2)$ for $\ddot{\mathbf{U}}$ and $\dot{\mathbf{U}}$. This method leads to an explicit procedure and a conditionally stable scheme. This scheme requires then the use of time step Δt smaller than a critical time step Δt_{cr} (See also section 3.3.2).

3.3. *Parameters for the computations*

3.3.1. *Loading*

Loading characteristics have been derived from experimental measurements conducted by van Bree *et al.* (1998), van Bree *et al.* (2000)) and Herlaar (2003). The work of these authors was dedicated to the investigation of the high-frequency response on physical models of the thorax that consist in a tissue simulant (gelatin or silicon gel) contained in a transparent container.

Pressure transducers used in the experiments of van Bree *et al.* (1998) on tissue simulant indicated that the amplitude of the wave associated with the high-frequency response is in the range 10-20 MPa and that its time duration is more or less 100 μs.

With the knowledge of the pressure amplitude on the axis of impact and of the—spherical—shape of the wave, one can build the pressure distribution to apply on the surface of the gelatin block that would yield the measured pressure wave front (inverse problem). The calculated pressure distribution can thus be used as a boundary condition in the FE model of thorax. From the measurements of van Bree *et al.* (1998), the pressure distribution is calculated as follows: the maximum amplitude is taken on the axis of impact and is set to 15 MPa in accordance with the values measured. Due to geometrical spreading, the pressure amplitude of a spherical wave decreases with distance from the source. The decreasing of the amplitude with distance from the axis of impact that serves as boundary conditions on layer 1 is approximated and discretized; Figure 3 shows the spatial distribution of pressure used along $(O, \mathbf{x}_1)$, the distribution is the same along $(O, \mathbf{x}_2)$. The pressure distribution applied at the surface of layer 1 yields a resultant force applied on the model of thorax of about 50 kN.

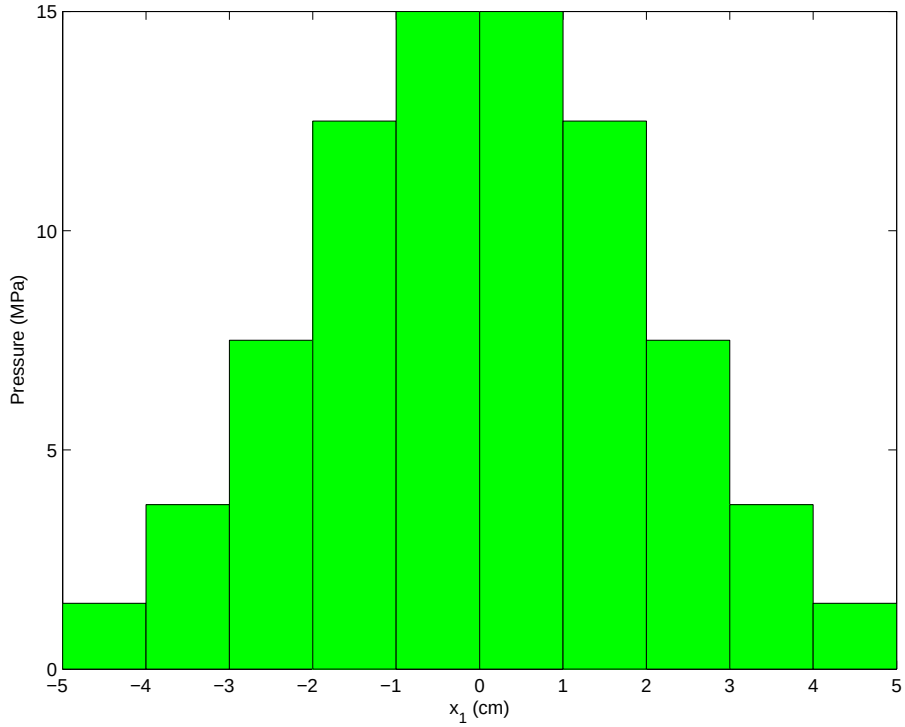

Figure 3. *Definition of the loading zones and load distribution*

In addition, to simplify the problem, the same time history of the loading is applied everywhere on the loaded surface; by doing this, the pressure wave generated in layer 1 has a plane wave front, and not a spherical wave front. This approximation is

justified because the distance of interest in the model are small (a few centimeters), in particular, only the response at points close to the axis of impact is considered.

The time history of typical impact waves show a steep wave front followed by an exponential decay. In order to simplify the analysis, the pressure history for the loading is taken to be a Blackman window function (van der Hijden, 1987) defined by:

$$\begin{cases} \phi(t) = 0 & \text{for} \quad t < 0 \\ \phi(t) = b_0 + b_1 \cos(2\pi t/T) & \\ \qquad +b_2 \cos(4\pi t/T) + b_3 \cos(6\pi t/T) & \text{for} \quad 0 \leq t \leq T \\ \phi(t) = 0 & \text{for} \quad t > T, \end{cases} \qquad [9]$$

where $b_0 = 0.35869$, $b_1 = -0.48829$, $b_2 = 0.14128$, $b_3 = -0.01168$, and where T is the duration of the pulse. This function, plotted in Figure 4, has the following beneficial features: it can be implemented using its analytical formula (making it easy to change the pulse duration); it is built as a sum of three Cosines functions of three different frequencies, so that its—discrete—spectrum is suitable to analysis; its duration, denoted by T, appears as a parameter which determines the frequency content.

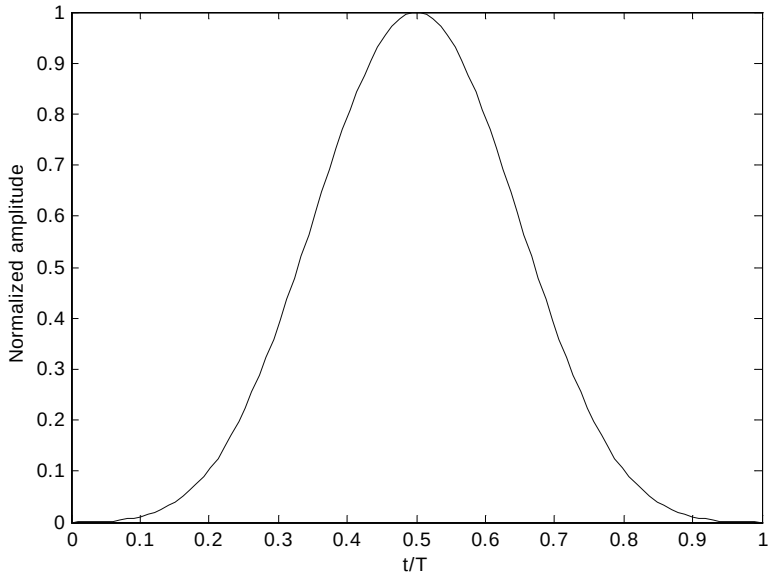

Figure 4. *Time history of the loading pressure applied on the surface of layer 1 (Blackman window of duration T)*

From experiments (van Bree *et al.*, 1998; van Bree *et al.*, 2000), it is known that the duration T of pressure wave is about 100 μs, this duration being variable between

experiments. In the present paper, results are shown for T=50, 100 and 200 μs; these durations where selected, in the range of what is commonly measured, so as to demonstrate different types of responses associated with high-frequency impact loading.

3.3.2. *Time step size*

The termination time T_t for the finite element runs was set at 200 and 500 μs depending on the loading duration. LS-DYNA is based on an explicit time integration scheme; the time step Δt to be used in the computations should be small enough so that information does not propagate across more than one element per time step (Hallquist, 2001). A critical time step size Δt_{cr} is computed for solid elements from

$$\Delta t_{cr} = \frac{L_e}{Q + \sqrt{Q^2 + c_L^2}}, \qquad [10]$$

where Q is function of the trace of the strain rate tensor $\dot{e} = \partial_t(\text{Tra } \boldsymbol{\epsilon})$

$$Q = \begin{cases} C_1 c_L + C_0 L_e \mid \dot{e} \mid & \text{for } \dot{e} < 0 \\ 0 & \text{for } \dot{e} \geq 0 \end{cases} \qquad [11]$$

where C_0 and C_1 are dimensionless constants ; The value defaults used by LS-DYNA are 1.5 and 0.06 respectively. The pressure wave speed c_L in the material is calculated with Eq. (4) and the characteristic length L_e for the hexahedral element with 8-nodes is obtained by

$$L_e = \frac{v_e}{A_e}, \qquad [12]$$

where v_e and A_e are respectively the element volume and the area of the largest side.

The time step size is taken from the minimum value over all elements

$$\Delta t = a \min\{\Delta t_1, \Delta t_2, ..., \Delta t_N\}, \qquad [13]$$

where N is the number of elements. For stability reasons the scale factor a is typically value of 0.9 or some smaller value.

In the present study, the solutions computed were not improved by taking a smaller time step than the default; therefore, the default setting was used in all computations.

4. Results

4.1. *Response of the thoracic wall*

In a first set of computations, the amplitude of the pressure applied on the thoracic wall model was kept constant while the duration of the pulse was varied: $T = 50, 100,$ or 200μs. With these loading conditions, the energy furnished to the structure increases with the pulse duration. Let A, B and C be three material points on the $\mathbf{x}_3$-axis: A is at the free surface of layer 1; B and C are at the interface between layers 2 and 3: B is on layer 2 and C on layer 3.

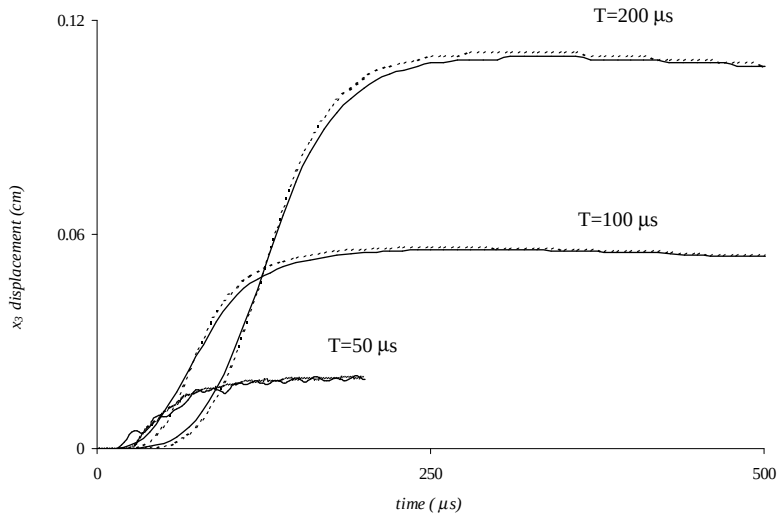

Figure 5. *Compilation of the displacements at points A and B (located on each side of the thoracic wall) for three pulse durations $T = 50\mu s$, $T = 100\mu s$ and $T = 200\mu s$. Continuous and dotted lines correspond to point A and B, respectively; the pulse duration corresponding to each curve is indicated on the figure*

Figure 5 shows the displacements at points A and B for the three pulses. The computation time window was taken shorter for the pulse $T = 50\mu$s to reduce the computation time but this has no influence on the analysis of the response since an asymptotic value is reached in the time window. As expected, the amplitude of the displacements increases with the amount of energy delivered to the structure (that is, with the pulse duration). For $T = 100$ μs and $T = 200$ μs, the responses at points A and B are very similar; basically, all the points in layers 1 and 2 have about the same motion. For $T = 50$ μs, the responses at points A and B follow a similar trend but oscillations typical of wave and vibration phenomena are superimposed to the global motion. These oscillations have a constant frequency and their period is very close to the travel time for a round trip of longitudinal waves in (layer 1+layer 2); the motion associated with the oscillations is the first compression/traction mode of vibration of the structure made of layers 1 and 2. Furthermore, the motion of (layer 1+layer 2) is almost not influenced by layer 3 because it is very compliant. For $T = 100$ μs, the maximum displacement of the lung surface is 560μm, which is of the order of the magnitude of the diameter of an alveolus in the lung. Note that the computed displacement is very small in comparison with the thickness of layers 2 and 3.

In Grimal *et al.* (2004), the finite element response of the thorax model was compared to the rigid body motion of a plate subjected to an equivalent loading. Results were in good agreement for a short time after impact; the better agreement was met for the shorter pulses.

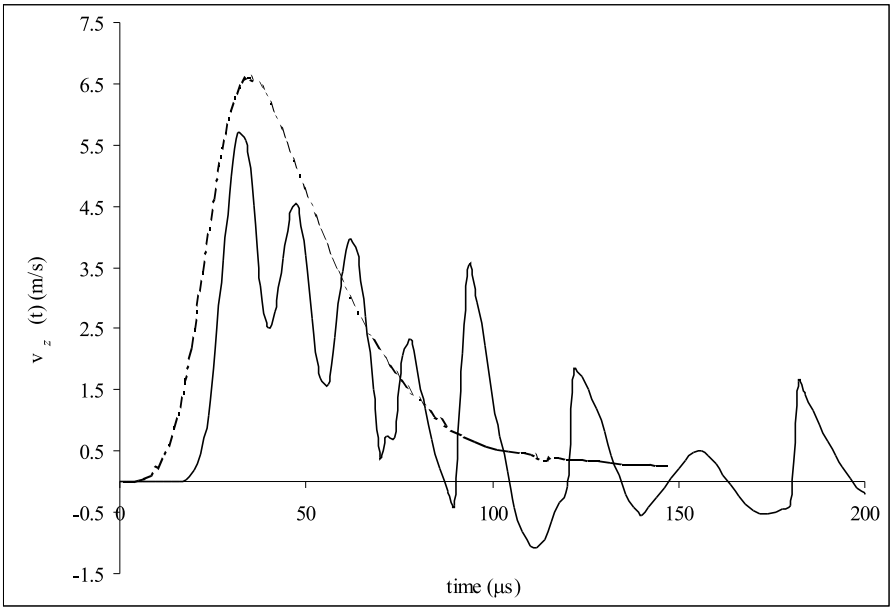

Figure 6. *Particle velocity at the layer-substrate interface computed with the finite element method (—) and calculated with the analytical solution from the classical plate theory (- -) for* $T = 50\ \mu s$

In figures 6-8, the response at point C is compared with the response of a homogeneous non-supported elastic plate, equivalent to (layer 1+layer 2). Free surface boundary conditions are assumed on both sides of the plate. The response of a plate, *with the assumptions of the classical plate theory*, subjected to an axisymmetric normal distributed uniform load, of resultant force P, is calculated with Eq. (14) which yields the response for a uniform load on a disc of radius a with center the origin of the Cartesian frame (Sneddon, 1951) (p. 141).

$$u_3(0,t) = \frac{P}{4\pi\sqrt{D\rho h}} \int_0^\infty \psi\left(t - \frac{a^2}{4b\zeta}\right) \frac{1-\cos(\zeta)}{\zeta^2} d\zeta, \qquad [14]$$

where u_3 denotes the displacement component along the $\mathbf{x}_3$-axis, $\psi(t)$ is the integral over time of the loading history, $D = (Eh^3)/(12(1-\nu^2))$ and $b = \sqrt{(D/\rho h)}$. In the FE model, the thoracic wall is made of two sublayers (representing muscle and bone), while using Eq. (14) an homogeneous medium must be defined: in the calculations,

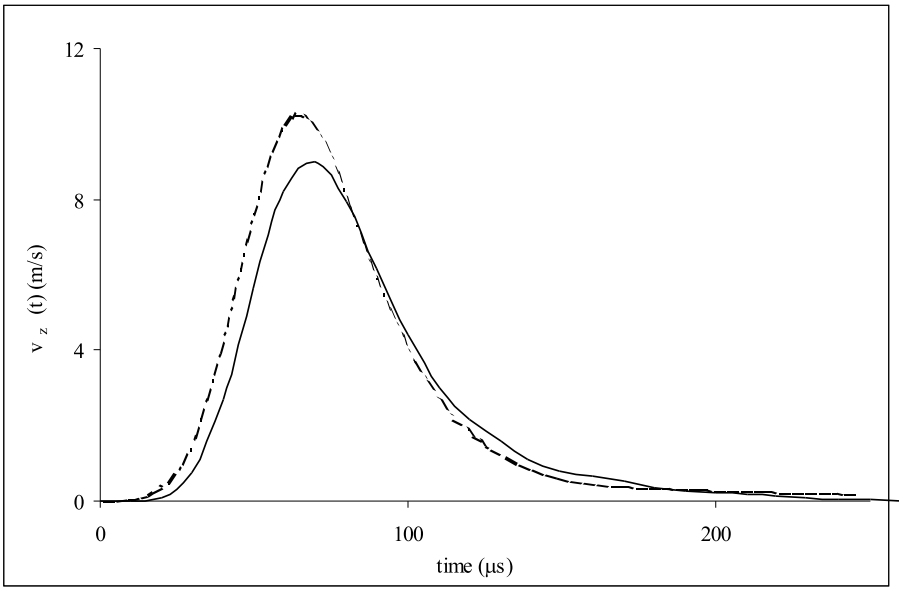

Figure 7. *Particle velocity at the layer-substrate interface computed with the finite element method (—) and calculated with the analytical solution from the classical plate theory (- -) for* $T = 100$ μs

we used $E = 2.28\ 10^9$ Pa, ν=0.4, h=2 cm and ρ=1750 kg m^{-3} for Young's modulus, Poisson's coefficient, thickness and mass density of the plate, respectively. It is manifest in figures 6-8 that the plate response is a very good approximation of the FE response, when the loading is "long" enough, that is, for an impulse duration of more than 100 μs.

Figure 9 gives $\sigma_{33}(t)$ at point B for the three pulses; the time data was translated using the theoretical arrival time of the pressure wave at point B, and then normalized with respect to the time duration of each pulse. This allows for the comparison of respective durations of the loading and the response. It is seen that for the longest pulse ($T = 200$ μs before normalization), the loading duration and the response duration are about the same. After the passage of the pulse, the TW is at rest. As the pulse shortens, the duration of the response increases. For $T = 50$ μs, an extended time elapses before point B returns to rest due to wave/vibration phenomena characterized by the oscillations of $\sigma_{33}(t)$. For this short pulse, energy is retained in the TW for a longer time before it is transmitted to layer 3.

The stress in the thickness of the TW (not represented) decreases from the free surface to the lung surface. From the mechanical point of view, this is required to satisfy the boundary conditions at the lung interface where the stress σ_{33} is small at

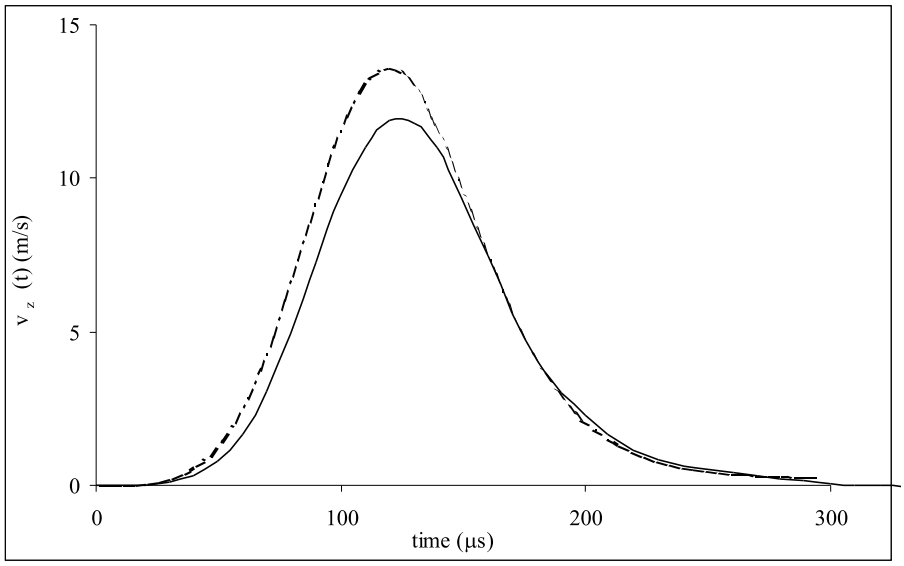

Figure 8. *Particle velocity at the layer-substrate interface computed with the finite element method (—) and calculated with the analytical solution from the classical plate theory (- -) for* $T = 200\ \mu s$

the interface due to the softness of the lung. During the passage of the pulse through the interface between layers 2 and 3, the two media remain in contact, furthermore σ_{33} is continuous across the interface, hence the stress σ_{33} at the surface of layer 3 that represents the lung is the same as shown in Figure 9.

4.2. *Wave phenomenon in the lung*

According to the elastic plane wave theory, the relation between normal stress and particle velocity is

$$\sigma_{33}(t) = \rho c_L v_3(t), \qquad [15]$$

where $v_3(t)$ is the particle velocity along the $\mathbf{x}_3$-axis. Equation (15) is readily obtained from the canonic form of the solution to the one dimensional wave equation—d'Alembert solution—, where the particle displacement is given by $u_3 = f(x_3 - c_L t)$, where f is an arbitrary function, c_L is the wave speed and x_3 denotes the position. This relation is valid for plane waves propagating in the direction $\mathbf{x}_3$ in an infinite medium. The stresses and velocities at point C computed by LS-DYNA deviate by less than 10% from the values calculated with Eq. (15). In contrast, the relation (15) is not true

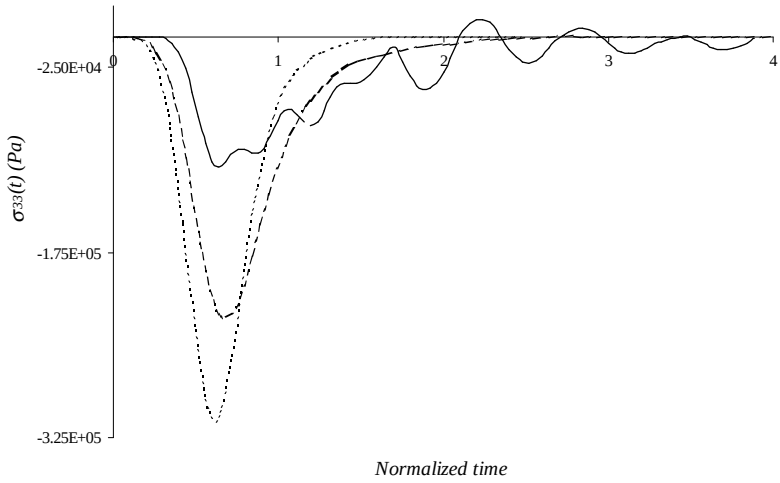

Figure 9. *$\sigma_{33}(t)$ at point B for $T = 50$ μs (continuous line), $T = 100$ μs (discontinuous line) and $T = 200$ μs (dotted line). Time is normalized: one unit on the abscissa corresponds to the duration of the pulse*

at points inside layers 1 and 2. This illustrates that a typical wave phenomenon in the lung is observed, as opposed to what is observed in the thoracic wall.

Figure 10 shows a typical FE result. The resultant velocity field 410 μs after the beginning of the loading ($T = 100$ μs) is shown; at this time, the energy of impact has entered the substrate and formed a wave.

4.3. *Energy delivered to the system and velocity at the lung surface*

Results presented above indicate that the displacements computed remain small for the loading amplitudes considered. Consequently, a linear relationship between the motion of the TW and the amplitude of the pressure applied on layer 1 is expected. As long as this property of linearity is valid, an estimate of the amplitude of the pressure to apply so as to generate a given velocity at point B can be calculated. For each pulse duration ($T = 50, 100$ and 200 μs), the appropriate amplitude of the pressure to apply on layer 1 so as to generate a velocity of 11 m s^{-1} at point C was determined; the maximum amplitude is found to be 29 MPa for the 50 μs pulse, 18 MPa for the 100 μs pulse and 15 MPa for the 200 μs pulse.

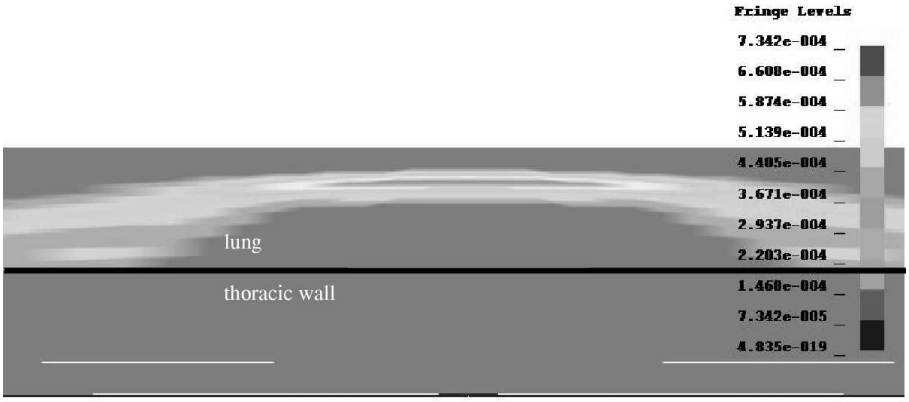

Figure 10. *Resultant velocity field at* $410\ \mu s$ *after the beginning of the loading for a loading duration of* $T = 100\ \mu s$*. Note the typical wave front, almost plane in the substrate (lung)*

The total energy delivered to the structure during the application of the load is obtained by post-processing LS-DYNA results; the total energy calculated is 4.7 J for $T = 50\ \mu$s, 12 J for $T = 100\ \mu$s and 20 J for $T = 200\ \mu$s. For each pulse duration, the energy transmitted to the three-layer structure, represents only a very small part of the incident energy of the 7.62 ball (3500 J); the rest of the incident energy is dissipated in the body armor and transmitted to the thorax by low-frequency mechanisms. However, the amount of energy associated with the high-frequency response generates relatively high velocities at the surface of layer 3 as compared to the velocity of longitudinal waves in the lung.

The comparison of the amount of energy delivered to the structure for each pulse duration indicates that the amount of energy required to generate a certain velocity at the lung surface is less for short pulses than for long pulses.

5. Discussion

5.1. *Mesh sensitivity*

Due to the very low wave speeds in the lung, the response in layer 3 is very sensitive to the mesh density. In this layer, the shortest wavelengths associated with the Blackman impulse of total duration $T = 100\ \mu$s are 1.3 mm and 0.7 mm for pressure and shear waves respectively. Within each element of the model, the quantity evaluated by the software (*e.g.*, displacements) is approximated by a function of a given class; the properties of a class of functions—and their ability to reproduce the spatial

variation of the quantity—depends on the type of element used. In order to accurately reproduce the evolution of the displacement within the material (at each time step), the size of an element should be less than the characteristic length over which the shape of the wave changes.

The size of the elements in the lung were chosen so that the spatial variation of the pulse associated with the highest frequency (30 kHz in this case) was computed. When the wave is propagating in the $\mathbf{x_3}$-direction, the spatial variations of the pulse are observed in the same direction. In contrast, the rate of variation of the displacement amplitude with respect to x_1 and x_2 is much less than for x_3. Therefore, the typical element size in the $\mathbf{x}_1$ and $\mathbf{x}_2$ directions was chosen larger than along $\mathbf{x}_3$. In Figure 11, the effect of using a coarse mesh is illustrated; $\sigma_{33}(t)$ for a receiver in layer 3 located on the $\mathbf{x}_3$-axis at a few millimeters above the interface is shown for different mesh densities.

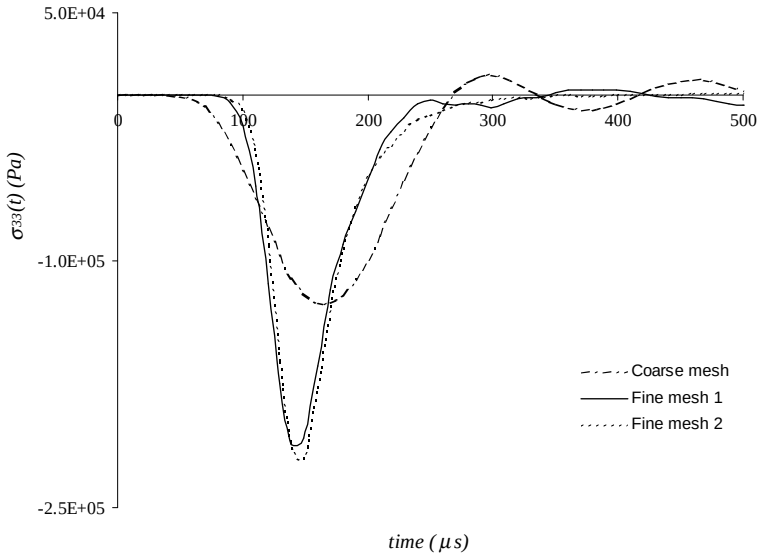

Figure 11. *Illustration of the mesh sensitivity: response in layer 3 (lung) for three meshes with different characteristic size of the elements (see Table 2)*

Mesh characteristics are given in Table 2, where ratios of the element length over minimal pressure and shear wavelengths are given. It was found that the ratio should be at least 0.3 to avoid dispersion of the pulse. Figure 11 reveals the low pass filter effect of a coarse mesh: as the mesh density decreases, oscillations typical of a dispersed pulse are observed at the end of the response; the response lasts longer and the rate of stress rise dramatically decreases, indicating that the high frequency content

has disappeared. The choice of the size of the elements in layer 1 and 2 requires less care since the wavelengths in these media are much larger than in the lung. In layer 3, the $\mathbf{x}_1$ and $\mathbf{x}_2$-dimensions of the smallest elements close to the $\mathbf{x}_3$-axis are 0.8 mm.

Table 2. *Element size and wavelengths in layer 3. The wavelengths λ_L and λ_S are respectively associated with c_L and c_S. Their values are obtained with a frequency of 30 kHz. The element length in the $\mathbf{x}_3$-direction (mm) is denoted by $d\ell_3$*

	$d\ell_3$	$d\ell_3/\lambda_L$	$d\ell_3/\lambda_S$
Coarse mesh	2	1.5	2.81
Fine mesh 1	0.4	0.3	0.56
Fine mesh 2	0.33	0.248	0.463

5.2. *Thoracic wall modelled as a plate*

There are three important consequences to the fact that the response calculated with the FE method —where the thoracic wall is modelled by two layers (muscle and bone) within the hypothesis of continuum mechanics— and the plate response— calculated within the hypothesis of classical plate theory— match well. 1) In the thoracic wall, the wave phenomena are negligible for $T > 100$ μs; the oscillations in the response for $T = 50$ μs observed in figure 6 are associated with the first mode of vibration of layers 1 and 2. In the rest of the paper, only impact durations $T > 100$ μs are considered. 2) The kinematics of the layer that represents the thoracic wall behaves much like if the substrate were absent. 3) With respect to the kinematics of the thoracic wall model, it is equivalent to calculate the response of a single layer (which properties are obtained upon homogenisation) than the response of two sublayers (as it is the case in the FE computations).

5.3. *Wave propagation in the lung*

Results presented in 4.2 demonstrate that a wave phenomenon in the lung occurs consecutive to the impulse loading. Hence the propagation of energy in the lung can be described in term of transmission/reflection at interfaces and focalization. Furthermore, since a quasi-plane wave is generated in the lung, the histories of the particle velocity or stress undergo little changes on the impact axis. Typical histories of particle velocities for the academic loading history considered (9) are plotted in figures 6-8.

Many authors have used the velocity at the surface of the lung as an injury criterion (Yen *et al.*, 1988; Viano *et al.*, 1988; Fung, 1990; Bir, 2000). This is consistent with our results since the velocity at the lung surface is directly related to the amplitude of the stress wave in the lung as pointed above.

5.4. *The proposed injury mechanism*

A "good" injury mechanism must account for the correlation between injury occurrence and an impact parameter established from experimental data. Basically, it is a succession of events relating some impact parameter(s) to local injury. The injury mechanism is useful in modeling as well as in experiment design and interpretation.

Following Cooper *et al.* (1996) we assume that local damage in the lung tissue is due to an excessive pressure jump Δp created between two adjacent alveoli during the passage of a wave. It is assumed that there exists a threshold for Δp above which alveoli are damaged.

Results of the previous subsection give the trend of the thorax response to a very short-duration pressure impulse on the thoracic wall. (The reader should keep in mind in the discussion that follows that no significant displacement of the body wall nor of the organs is involved and that displacement-related injuries are out of the scope of this study.) Following Grimal *et al.* (2005), the lung injury mechanism can be described as follows. i) The transmission of the impact wave from the body armor to the thorax corresponds to the application of a distributed and time-dependant pressure on the body wall. ii) Due to this load, the thoracic wall is set in motion like a homogeneous, non-supported plate. iii) This motion creates an almost plane longitudinal wave in the lung which history is close to the history of the applied loading. Hence the particle velocity at a point in the lung is of the order of magnitude of the particle velocity at the interface, that is, of the thoracic wall velocity. In BABT-like impacts, this mechanism of energy transmission is possibly the cause of part of the pulmonary injury: the particle acceleration in the lung can generate a significant local pressure differential.

5.5. *Limitations*

The model of thorax investigated has many limitations. It is limited to the analysis of the transmission of the impact energy through the thoracic wall into the lung tissue, beneath the impact point. It is clearly unable to predict occurrence of injury at a precise anatomic location of the lung. The modelling philosophy adopted consisted in keeping only the main geometric features of the thorax (under the impact point). In this simple configuration, the relative importance of the different parameters that govern the behavior of the model show up as clearly as possible.

5.6. *Computational difficulties*

Some specific numerical problems showed up in the investigation of the idealized thorax model. The mesh sensitivity study has revealed that the maximum element size, in layer 3 (lung), to use for the computation of the response to a 100 μs duration impact, is 0.5 mm (for hexahedral elements with 8-nodes). The total number of

elements required to calculate the propagation of a 100 μs pulse in entire 3D model of lung would be enormous; hence an alternate solution strategy is required to solve this problem. Another numerical problem may occur when the load amplitude is so large that the thoracic wall velocity reaches the value of the wave speed in the lung (about 40 m s^{-1}); a shock wave will be generated and specific modelling should then be considered.

6. Conclusion

The response of an idealized model of thorax to loadings of duration around 100 μs has been investigated with the finite element method. The thoracic wall is found to behave like a homogeneous plate whereas, in the lung, the response is described in terms of waves. Many authors have suspected wave phenomena to be at work in lung injury mechanisms following high-velocity loadings of the thorax. Here, we give a sequence of events that may explain part of the observed lung damage.

Quantitative information on the thorax response has been obtained. These results need to be validated by experiments on physical and animal models.

Acknowledgements

The authors would like to thank the “Délégation Générale pour l’Armement” of the Minister of Defense of France for supporting this work.

7. References

Bir C., The evaluation of blunt ballistic impacts of the thorax, PhD thesis, Wayne State University, Detroit, Michigan, 2000.

Bush I., Challener S., « Finite element modelling of non-penetrating thoracic impact », *Proceedings of the International Research Council on the Biomechanics of Impact (IRCOBI), Bergish-gladbach*, p. 227-238, 1988.

Cannon L., Tam W., « The development of a physical model of non-penetrating ballistic injury », *19^{th} International Symposium of Ballistics, 7-11 May 2001, Interlaken, Switzerland*, p. 885-888, 2001.

Cooper G., Maynard R., « An experimental investigation of the biokinetic principles governing non-penetrating impact on the chest and the influence of the rate of body wall distortion upon the severity of lung injury », *Proceedings of the International Research Council on the Biomechanics of Impact (IRCOBI), Zürich*, p. 331-342, 1986.

Cooper G., Pearce B., Sedman A., Bush I., Oakley C., « Experimental evaluation of a rig to simulate the response of the thorax to blast loading », *The Journal of Trauma*, vol. 40, p. S38-S41, 1996.

Cooper G., Townend D., Cater S., Pearce B., « The role of stress waves in thoracic visceral injury from blast loading: modification of stress transmission by foams and high-density materials », *Journal of Biomechanics*, vol. 24, p. 273-295, 1991.

Cooper J., Pearce B., Stainer M., Maynard R., « The biomechanical response of the thorax to nonpenetrating impact with particular reference to cardiac injuries », *The Journal of Trauma – Injury Infection and Critical Care*, vol. 22, p. 994-1008, 1982.

Fung Y., *Biomechanics: motion, flow, stress, and growth*, Springer-Verlag, New-York, 1990.

Fung Y., *Biomechanics; mechanical properties of living tissues*, Springer-Verlag, New-York, 1993.

Grimal Q., Gama B., Naïli S., Watzky A., Gillespie J., « Finite element study of high-speed blunt impact on thorax: linear elastic considerations », *International Journal of Impact Engineering*, vol. 30, p. 665-683, 2004.

Grimal Q., Naïli S., Watzky A., « A high-frequency lung injury mechanism in blunt thoracic impact », *Journal of Biomechanic*, vol. 38, n° 6, p. 1247-1254, 2005.

Hallquist J., LS-DYNA theoretical manual and keyword user's manual, Technical report, Livermore Software Technology Corporation, 2001.

Herlaar K., Optical pressure measurement methods at impact loading in a tissue simulant behind armour, PhD thesis, Faculty of Applied Sciences, Delft University of Technology, Delft, the Netherlands. Munition Effects and Ballistic Protection Group, TNO Prins Maurits Laboratory, Rijswijk, the Netherlands, 2003.

Jahed M., Lai-fook S., Bhagat P., Kraman S., « Propagation of stress waves in inflated sheep lungs », *Journal of Applied Physiology*, vol. 66, p. 2675-2680, 1989.

National Library of Medicine, « Visible Human Project », 2003. WEB page http://www.nlm.nih.gov/research/visible/.

Raftenberg M., Response of the Wayne State Thorax Model with fabric vest to a 9-mm bullet, Technical Report n° ARL-TR-2897, Army Research Laboratory, 2003.

Raftenberg M., DeMaio M., Parks S., Blethen W., Carlson T., Mackiewicz J., « Blunt trauma from nonperforating impact on fabric armor », *Proceedings of the 25th Annual Meeting of the American Society of Biomechanics*, 2001.

Sarron J., « La modélisation numérique dans la définition de nouvelles protections individuelles antibalistiques », *L'Armement (revue de la Délégation Générale pour l'Armement)*, vol. 76, p. 54-61, 2001.

Sarron J., Da Cunha J., Caillou J., Allain J., « Dynamic cone development in aramid plate, modeling of rear effects for individual protection », *Proceedings of the PAM Users Conference in Europe EuroPAM, Nantes, France*, October, 2000.

Sneddon I., *Fourier transforms*, International Series in Pure and Applied Mathematics, first edition edn, McGraw-Hill Book Company, Inc., 1951.

Stuhmiller J., Chuong C., Phillips Y., Dodd K., « Computer modeling of thoracic response to blast », *Journal of Trauma – Injury Infection and Critical Care*, vol. 28, p. S132-S139, 1988.

van Bree J., Gotts P., « The 'twin peaks' of BABT », *Proceedings of the Personal Armour Systems Symposium 2000. Colchester, UK. 5-8 Septembre*, 2000.

van Bree J., van der Heiden N., « Behind armour blunt trauma analysis of compression waves », *Proceedings of the Personal Armour Systems Symposium 1998. Colchester, UK. 8-11 Septembre*, p. 433-440, 1998.

van der Hijden J., *Propagation of transient elastic waves in stratified anisotropic media*, vol. 32 of *Applied Mathematics and Mechanics*, North Holland, Elsevier Science Publishers, Amsterdam, 1987.

Vawter D., « A finite element model for macroscopic deformation of the lung », *Journal of Biomechanical Engineering*, vol. 102, p. 1-7, 1980.

Vawter D., Fung Y., West J., « Constitutive equation of lung tissue elasticity », *Journal of Biomechanical Engineering*, vol. 101, p. 38-45, 1979.

Viano D., King A., Melvin J., Weber K., « Injury biomechanics research: an essential element in the prevention of trauma », *Journal of Biomechanics*, vol. 22, p. 403-41, 1989.

Viano D., Lau I., « A viscous tolerance criterion for soft tissue injury assesment », *Journal of Biomechanics*, vol. 21, p. 387-399, 1988.

Wang H., Development of a side impact finite element human thoracic model, PhD thesis, Wayne State University, Detroit, 1995.

Yen R., Fung Y., Ho H., Butterman G., « Speed of stress wave propagation in lung », *J. Appl. Physiol.*, vol. 61, n° 2, p. 701-705, 1986.

Yen R., Fung Y., Liu S., « Trauma of the lung due to impact load », *Journal of Biomechanics*, vol. 21, p. 745-753, 1988.